Algal biomass particle size and self-bonding effects on cement composites

Brandon Tyler Lou

A thesis

submitted in partial fulfillment of the

requirements for the degree of

Master of Science

University of Washington

2023

Committee:

Eleftheria Roumeli

Dwayne Arola

Program Authorized to Offer Degree:

Materials Science and Engineering

University of Washington

Abstract

Algal biomass particle size and self-bonding effects on cement composites

Brandon Tyler Lou

Chair of the Supervisory Committee:

Eleftheria Roumeli

Materials Science and Engineering

Cement is a large contributor to carbon dioxide (CO_2) emissions, and there is ongoing research to reduce this impact. Algal biomass, in various forms, is studied for potential applications in many industrial industries including the cement industry. This is large in part due to the wide availability of the abundant organic biomass in coastal marine regions. Prior literature has seen *Arthrospira (Spirulina) platensis* microalgae integrated with Ordinary Portland cement (OPC). This work explores the incorporation of raw and self-bonded algal biomatter to see the impact on the cement composites. The known effect of particle size is also further studied. We respectively incorporate microalgae (*Arthrospira platensis*) spirulina and macroalgae (*Ulva expensa*) in OPC at concentrations of 1%, 5%, and 10%. This is completed at three distinct particle size ranges as well as for raw and self-bonded biomass. We observe their effects on the mechanical strength, hydration product

formation, and micromorphology of the composites through compression testing, thermogravimetric analysis and scanning electron microscopy, respectively. Spirulina microalgae composites performed as expected with a drastic reduction in compressive strength at 5% concentration while ulva macroalgae experiences a decrease in performance with increasing concentration, but the effect is not significant until 10% and is less dramatic than what is observed in the spirulina. Smaller particle sizes in the ulva composites are on average 1.49 times stronger than their large particle size counterparts, this factor is similar in spirulina but again at relatively much lower strengths. Self-bonding has the opposite effects on the microalgae and macroalgae systems, where self-bonding enhances the strength of ulva-cement composites up to 224%. This work furthers the investigation of whole algal biomass as additions to cement, with the intention of finding methods to reduce the detrimental environmental impact associated with cement production.

Table of Contents

1. Introduction

1.1 Cement

Concrete is the most popular construction material on the planet, used for various construction applications such as buildings, highways, and bridges. Concrete is a composite consisting of 60-75% aggregates (both coarse and fine), water (the amount depending on the water-cement (w/c) ratio), and cement (7-15%) [1]. Cement is the binder for concrete composites and is responsible for the development of mechanical strength. Cement production is associated with an estimated 0.93 kg of CO_2 emissions for every kilogram of powder produced. It is well documented that the cement industry alone contributes to 5-8% of global greenhouse gas emissions [2]–[6]. The calcination process accounts for over 50% of these emissions [7], while around 40% is attributed to fueling combustion for calcination, and ~5% to electricity and transport [8].

Ordinary Portland cement (OPC) is the most popular general-use cement globally, accounting for over 85% of US cement shipments in 2014 [9]. After 28 days of curing and the OPC has reached its hardened state, the material will have 80-85% of its achievable strength [10] and has reached “steady-state.” Once at steady-state, the strength development enters a plateau where strength increases in a less accelerated manner than initial (< 7) days. Because of this strength development behavior, the 7 and 28-day mechanical strength of cement composites are commonly reported. With a w/c ratio of 0.35, 28-day OPC has a compressive strength of 57.9 MPa [11]. It is worth noting that a

compressive strength of 21 MPa is the typical requirement for light commercial and residential concrete applications [12], with strength requirements for structural elements of larger structures reaching over 41 MPa [13].

There are various reactions within cement during the curing period that contribute to the strength development of cement composites. Cement is composed of minerals which react with the water introduced during mixing, and these strengthening reactions are therefore denoted “hydration” reactions. **Equations 1-3** below present three primary reactions, with their hydration products highlighted in the SEM image shown in **Figure 1**. **Equation 1** shows the tricalcium culminate in the cement powder reacts to form $Ca_6Al_2(SO_4)_3(OH)_{12}\cdot 26H_2O$ (ettringite), which are high aspect ratio, needle-like formations that make up around 15% of the steady-state cement; this is the first generated product in the hydration reactions. While ettringite does not contribute to the strength of the cement composite [14], [15]. Generating from tricalcium silicate (alite) and dicalcium silicate (belite) as shown in **Equations 2-3**, $CaO_x\cdot SiO_2\cdot (H_2O)_n$, more commonly referred to as calcium silicate hydrate (C-S-H), is an amorphous structure composed of fibers with smaller aspect ratio than ettringite; this hydration product makes up over 60% of the steady-state cement and contributes greatly to the overall strength [14], [16]. Finally, $Ca(OH)_2$ (calcium hydroxide, portlandite) is a platelike hydration product that makes up around 20% of the steady-state cement [14].

$$3CaO\cdot Al_2O_3 + 3[CaSO_4\cdot 2H_2O] + 24H_2O \rightarrow \text{heat} + [Ca_6Al_2(SO_4)_3(OH)_{12}\cdot 26H_2O] \quad (1)$$

$$Ca_3SiO_4 + ((3 \text{ or } 2)(x\text{-}n))H_2O \rightarrow CaO_x{\cdot}SiO_2{\cdot}\ (H_2O)_n + 3[Ca(OH)_2] \quad (2)$$

$$Ca_2SiO_5 + 4H_2O \rightarrow 3CaO{\cdot}SiO_2{\cdot}H_2O + Ca(OH)_2 \quad (3)$$

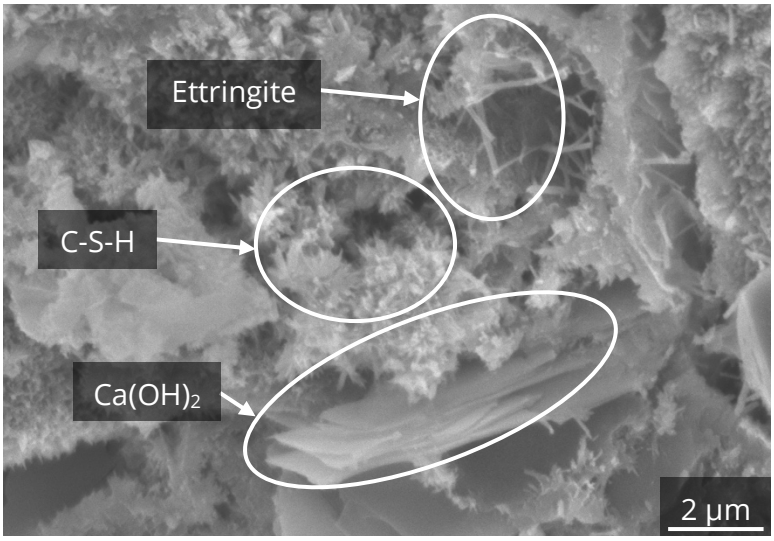

Figure 1. SEM micrograph of cement composite to visualize various hydration products.

Due to the detrimental environmental impact of cement powder production, there are ongoing efforts to try and reduce the greenhouse gas emissions related to this process. Utilizing industrial byproducts as admixtures and additives to concrete such as silica fumes, fly ash, and blast furnace slag are common for applications promoting late-age performance through pozzolanic reactions [17]–[20]. Natural additives are also utilized with the intention of enhancing certain properties of the composite while serving as more eco-friendly solutions; examples include bamboo [21], nanocellulose [22], and hemp [23]. Therefore, both the environmental impact and mechanical performance are considerations for additives in a cement composite. Additionally, the strength of the interface carries a significant impact towards the mechanical performance of the overall composite [24], [25]

as weaker interfaces can lead to a defect-driven effect [26]. In concrete, the interface between aggregates and cement, referred to as the “transition zone,” is the weakest region due to the increased amount of water [27]; furthermore, this transition zone is weaker due in part to the increased concentration of calcium hydroxide crystals near aggregates preventing C-S-H growth and subsequent matrix densification [28]–[30].

1.2 Algal biomass as an additive

Algae is a widely abundant biomass seen often as waste due to its proliferation in coastal regions with no standard industrial application [31]. However, algae is well-studied for its potential applications such as packaging film, fibers in polymer composites, and biodiesel fuel in various industries [31]–[35]. Due to the advantage of rapid growth rates and low land use requirements, utilizing algae in cementitious materials has become an emerging field. In the past 25 years, algae-cement composites have been investigated for potential enhancements in workability [36], self-healing of cracks [37]–[39], and mechanical performance [40]. The algae’s ability to sequester carbon [41] also provides a potential benefit as an additive for cement in regards to the negative environmental impact of cement production. Both macro- and micro-algae have been previously studied for their potential benefits to composite systems [31], [34], [42]. Other than using the extracted algal biomatter, there is previous work exploring microalgae as filler in cement composites that revealed the hindrance effect of chlorella and spirulina on cement hydration reactions at high concentration (> 5 wt%) by Lin et al. [43], and the retardation effect of chlorella at low concentration (< 3 wt%) by Chen et al. [44]. Ramasubramani et al. and Achenza et al. have

previously explored macroalgae applications [45], [46], but a well-developed understanding of the mechanisms is not defined. In this current work *Arthrospira (Spirulina) platensis (microalgae)* and *Ulva expensa (ulva) (macroalgae)* are respectively introduced to the cement matrix to compare the effects on the strength development, the steady-state compressive strength, and the cement hydration reactions.

1.3 Particle size effect and self-bonding

Regarding OPC, it is understood that the particle size shares an inverse relationship with the percentage of hydrated product, and therefore the final mechanical strength. This relationship is explained by the water penetration at smaller particle sizes allowing for an increase in hydration reactions to occur [47]. Previous works of microalgae as additives in cement composites used raw chlorella powder [43] and ground chlorella pellets [44], which showed different mechanical properties respectively while the effect of particle size has not been studies in detail. The hydrophilic feature of algal biomass is noted to have a potential impact on the cement-biomass interface, which can hinder the mechanical performance [27]. Furthermore, the surface area to volume ratio of a particle is directly proportional to its surface energy [48], which is well studied at the nanoscale in particular. Effectively decreasing the particle size of the biomass will increase the surface area to volume ratio, which could prove preferential for interface development and mechanical performance as well.

Pressing algae at high temperature and pressure increases the number of both covalent and hydrogen bonding, and a processable thermoplastic is obtained with mechanical properties more desirable than the raw biomass; this process classifies the biomass as “self-bonded.” The compressive strength of pure self-bonded spirulina is reported at 76 MPa by Iyer et al., suggesting the development of strong bonds between the spirulina material [49]. The self-bonding of biomass, both spirulina and ulva, is investigated further in this work to observe the effect on mechanical performance of cement composites. The importance of the interface energy between filler and matrix is noted, and microstructural analysis will be implemented to compare the interfaces between the cement matrix and varying biomasses.

The following experiment aims to integrate algal biomass in different forms with the OPC matrix. Integration of the algal biomass will be performed with both spirulina and ulva at three discrete particle sizes; as previously discussed, particle size is expected to have an inverse relationship with the mechanical performance of the cement composites. The effect of self-bonding the biomass as a pre-processing condition is also explored with the hopes of seeing a correlation to mechanical performance. Further understanding the effects of particle size and self-bonding of both micro and macroalgae on the mechanical strength of cement composites will continue the ongoing research for utilizing algal biomass in applications for structural materials to reduce carbon emissions of the cement industry.

2. Materials and Methods

2.1 Materials

Type I-II OPC was obtained in a powder form from Sakrete (Charlotte, NC, USA) and meets ASTM C150 [50] standards (**Figure 2a**). The chemical composition of this cement powder is shown in **Table 1**. Spirulina (nuts.com, Cranford, NJ, USA) microalgae was commercially obtained in a powder form with a density of around 1.2 g/cm^3 (**Figure 2b**). Characterized by SEM images and ImageJ, the particle sizes of the specific materials used in this experiment are 5-20 μm for cement and 20-40 μm for spirulina's chain of cells [43]. Ulva (**Figure 2c**), a form of green macroalgae, was provided by Pacific Northwest National Laboratories (PNNL, Richland, WA, USA) in the form of freeze-dried flakes on the centimeter scale. Noting that algal growth environment affects subsequent composition, the specific ulva used in this experiment was grown in a high-flow current environment.

Figure 2. Materials used in this study. OPC (a), (b) freeze-dried spirulina, and (c) freeze-dried high-flow ulva in their unprocessed powder forms.

Table 1. Oxide content (wt %) of cement powder used in this experiment [43].

CaO	SiO_2	SO_3	Al_2O_3	MgO	Fe_2O_3	K_2O	Na_2O
67.14	14.00	9.68	3.51	1.70	2.81	0.89	0.28

2.2 Self-bonding

Biomass was self-bonded via hot-pressing to observe the effect of this preprocessing step. The ulva in supply was provided as inhomogeneous flakes, so 8-11 g of biomass is ground with coffee grinding (Hamilton Beach Model No. 80335RV, Glen Allen, VA, USA) for 60 seconds to both decrease the particle size and homogenize the powder before hot-pressing. One gram ground algal biomass was placed in steel bar-shaped mold shown in **Figure 3a** and were then hot-pressed at a desired temperature of 140 °C, and a target pressure of one MPa for a duration of five minutes using the TMAX-SYP-600 (TMAXCN, Xiamen, Fujian, China) shown in **Figure 3b**. The result was a bar of the self-bonded biomass as shown in **Figure 3c**, which was ground into different particle sizes as a bio-additive.

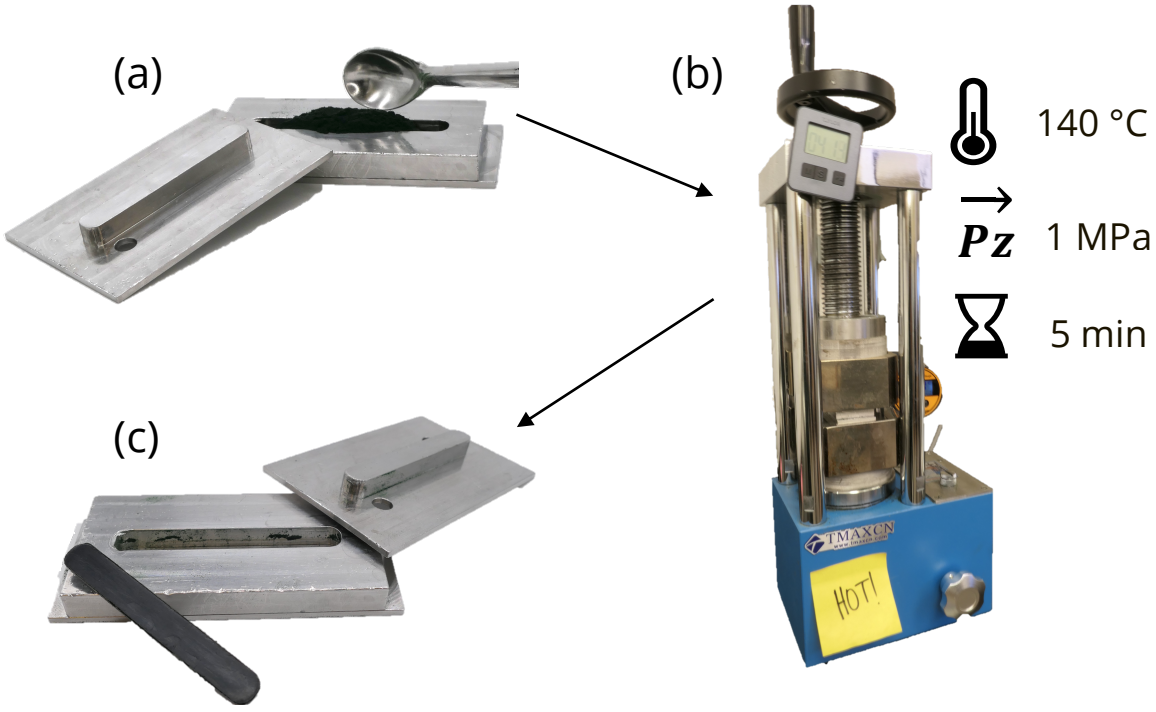

Figure 3. Manufacturing self-bonded biomass. (a) add raw powder to custom mold, (b) subject mold to hot pressing under given conditions, and (c) remove the self-bonded powder for additional processing.

2.3 Particle size processing

For both the spirulina and the ulva, there were three discrete particle size ranges desired for this experiment. The procedures for the two larger particle size ranges and the smallest differ slightly. Biomass (excluding virgin spirulina) was ground using a hand grinder with adjustable fineness, starting at a coarser setting, and increasing the fineness as necessary. Using a sieve tower that meets ASTM E-11 [51] specifications, biomass was passed through the sieves iteratively with additional grinding between passes until enough biomass at each particle size range was obtained. The largest particle size range was the biomass that fell between Mesh No. 35 and 100 (500 μm and 150 μm, large), while the next range between Mesh No. 100 and 325 (150 μm and 45 μm, medium). Representative images of biomass powder at the medium and large particle size ranges are shown in **Figure 4a-d**, with correlating particle size distributions of these ranges presented in **Figure 4g**.

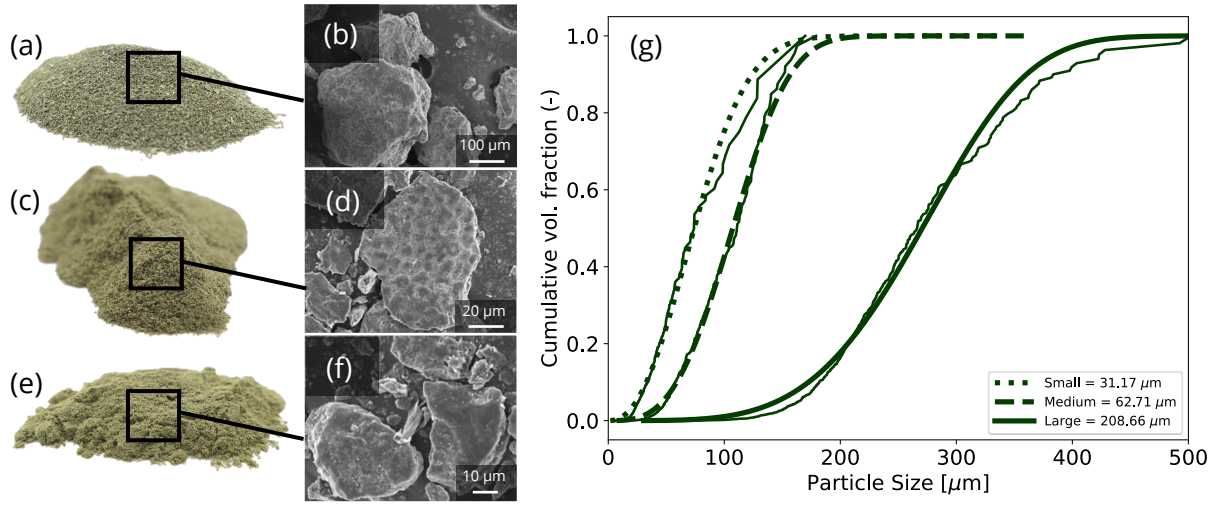

Figure 4. Powder size analysis. Photographs and corresponding SEM images of (a-b) large self-bonded ulva, (c-d) medium self-bonded ulva, and (e-f) small self-bonded ulva. (g) Corresponding Weibull distribution curves of powders.

The smallest particle size was achieved via milling. For this step, biomass was first processed to a particle size range akin to the medium range described above. Virgin ulva was ball-milled at 500 rpm for 20 minutes using a Vertical High Energy Planetary Ball Mill (MSE Supplies, Tuscon, AZ), while both the self-bonded ulva and self-bonded spirulina were speed-milled at 2500 rpm for 60 seconds using the SpeedMixer grinding accessory (Form-Tech Scientific, Toronto, Canada) with a speed mixer (DAC 330-100 PRO; FlakTek SpeedMixer, Landrum, SC). A representative image of the smallest particle size biomass is pictured in **Figure 4e-f** and the correlated particle size distribution in **Figure 4g**. Due to processing constraints, raw spirulina was not altered to the larger particle size ranges, and the out-of-bag particle size aligned with the smallest particle size range.

2.4 Sample fabrication

In this experiment, samples of 1, 5 and 10 wt% biomass were introduced to the cement composites, where the weight percent is the ratio of the mass of biomass powder to the mass of total dry powders used (biomass and cement summation). For 1 and 5%, a water-cement ratio of 0.40 was used while 0.50 was used for 10% samples due to workability constraints at high concentration. The dry powders were placed into a speed mixer (DAC 330-100 PRO; FlakTek SpeedMixer, Landrum, SC) and mixed at 1500 rpm for 30 seconds, with the resultant powder depicted in **Figure 5a**. The DI water was then added to the dry powders, and this was mixed in the speed mixer at 1500 rpm for 45 seconds four total times with 15 second resting intervals in between. After sufficient mixing, the cement slurries were cast to VytaFlex 30 urethane rubber (Smooth-On, Macungie, PA) molds

(**Figure 5b**) of cubes measuring 10 mm in each dimension; molds 8 mm in each dimension were used for both control and 1% biomass samples due to load cell limitations. All molds were coated with AquaRelease 75 (Mann Release Technologies, Macungie, PA) concrete water-based release agent prior to casting the slurry to prevent samples adhesion to the molds. When casting the slurry, the molds rested on a vibrating table (Buffalo No. 1A Vibrator; Syosset, NY) while the slurry is cast. Once the cement slurries fill the molds halfway, a steel spatula rods the mixture to remove entrapped air bubbles. This rodding is repeated when the molds are filled by the slurry. The resultant samples (**Figure 5c**) are then covered with a plastic film to minimize water evaporation and left to set for 24 hours in a humidity chamber held to ~90% RH +/- 5% and 23 +/- 1 °C. For each biomass concentration, a minimum of 32 samples were fabricated. This was completed for virgin

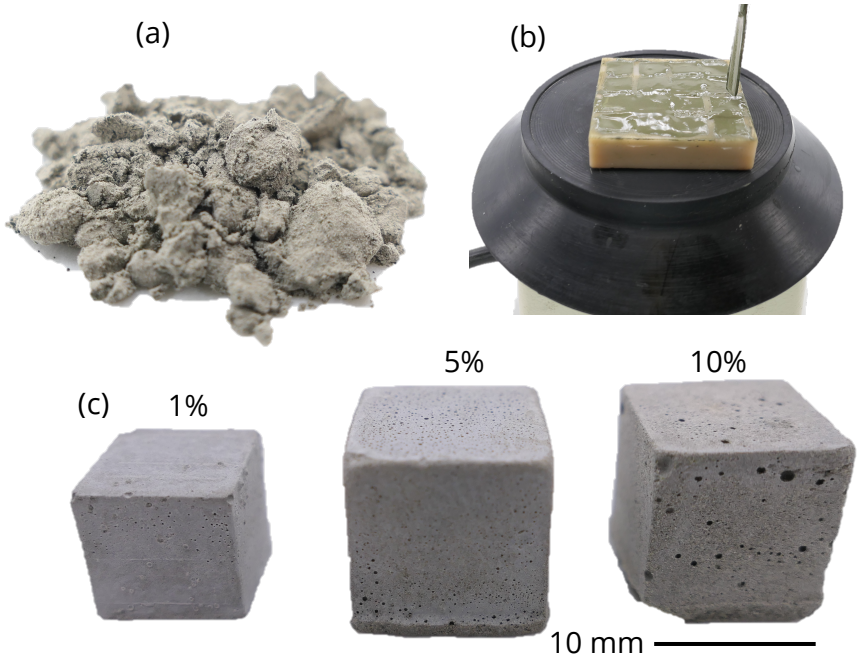

Figure 5. Stages of sample fabrication. (a) mixed cement and biomass powder, (b) wet slurry casted in rubber mold on vibrating table being rodded, and (c) 1%, 5%, and 10% (left to right) hardened samples with scalebar.

spirulina at its out-of-bag particle size as well as for self-bonded spirulina, raw ulva, and self-bonded ulva at small, medium, and large particle size ranges.

After the designated 24 hours of initial setting in the rubber molds, the cement samples were removed from their molds and returned to the humidity chamber to continue the hardening/curing process for the duration of the experiment.

2.5 Compression testing

Compression testing was conducted on the cement samples to obtain the stress-strain curves and subsequently the ultimate compressive strength. Samples were mechanically tested on days 1, 3, 7, 14, and 28 to develop an understanding of the strength development in each sample and how it compares to that of pure cement. Five samples from each set of samples were tested at each time point. Sample surface abnormalities and defects were removed using 400 grit sandpaper prior to measuring each side of the cubic structures using digital calipers, with the largest dimension designated as the height. Sample mass was recorded using a digital scale (Shimadzu UX220H; Kyoto, Japan). The testing was conducted using a universal load frame (Autograph AGS-X 10kN, Shimadzu Scientific Instruments, Columbia, MD, USA) attached with a 5 kN load cell and flat platens. All conducted tests were in accordance with ASTM C109/109M [52]. The measured force (F) and displacement (L) were normalized by their cross-sectional area (A) and initial height (L_0) respectively to acquire the stress (σ) and strain (ε), as visualized in **Equations 4 and 5**. This was then analyzed further to find the maximum stress, which is interpreted as the ultimate compressive strength (σ_c).

$$\sigma = \frac{F}{A} \tag{4}$$

$$\varepsilon = \frac{L}{L_0} \tag{5}$$

2.6 Scanning electron microscopy (SEM) and energy dispersive spectroscopy (EDS)

SEM analysis was conducted to analyze the micromorphology of the samples. The micromorphology will give insights to the integration of the biomass with the cement matrix, the dispersion of the biomass throughout the matrix, and a qualitative perspective of the effect the biomass will have on the hydration products of cement. SEM was conducted on samples at both day 7 and day 28 for early and late strength comparisons. Imaged surfaces were inner areas of samples exposed after compression testing, therefore allowing us to view the fracture surface. Prior to imaging, the non-conductive cement samples were sputter-coated with a thin layer of conductive palladium/gold with a current of 15-17 mA for 45 seconds to ensure image quality and prevent charging. SEM for this experiment was conducted with the JSM-6010 Plus/LA with a voltage of 10 kV, initial working distance of 10 mm, and spot size 30 (JEOL, Peabody, MA, USA). SEM was also conducted for each particle size range used in this experiment, and these images were then processed via ImageJ [53] to find the average particle size and distributions.

For this experiment, samples were analyzed via EDS at steady state (≥ 28 days), ideally at the interface between a biomass particle and the cement matrix. Probing this area of samples allows for analysis of any chemical alterations that may be occurring in the

composite due to the biomass. Manual probing was used, meaning the user chooses points for examination. This was completed on the same SEM used for microstructural analysis, but higher voltages (12-15 kV) and larger spot sizes (50-60) were implemented to increase the intensity of the signal. Note that the sputter coated elements (palladium and gold) are neglected for analysis as they are not expected in the cement composites.

2.7 Thermogravimetric analysis (TGA)

TGA observes the change in mass of a sample as a temperature regiment is applied and can observe relative different amounts of hydration products at steady state. The TGA for this experiment was conducted using a TA Instruments D550 (New Castle, DE, USA). Cement composites at steady state were grinded to a powder using a mortar and pestle, and 5-10 mg were placed in platinum crucibles for further analysis. The heating regiment first went from ambient temperature to 140 °C at a heating rate of 10 °C/min. After holding at 140 °C for 25 minutes to fully evaporate entrapped water in samples, the temperature was increased to 1000 °C at a rate of 10 °C/min and held at 1000 °C for 30 minutes. Inert nitrogen flowed throughout the duration of the experiment with a 20 mL / min flow rate.

The temperature regiment at the beginning (room temperature to 140 °C) allows for any entrapped water to be evaporated before the rest of the test to ensure no mass loss is mistaken for water loss; this can be designated as the initial portion with the rest of the test serving as the primary portion. For this report, the primary portions of the TGA curves are compared between one another to observe differences in cement hydration products involving $Ca(OH)_2$ and $CaCO_3$.

3. Results and Discussion

3.1 Effects of ulva macroalgae on cement composites

We first look at the effect of macroalgae on the cement composites. This will be assessed by isolating each characterization method for discussion: first mechanical results, followed by thermal degradation profiles, and concluding with micromorphological assessments. The effects of these variables are not directly transferrable to the microalgae studied, which will be discussed separately in *Section 3.2* for microalgae.

3.1.1 Mechanical Results

The steady-state mechanical performance is considered in below where **Figure 6a** shows the 28-day σ_c of raw ulva cement composites and **Figure 6b** shows such for self-bonded cement composites. The black dashed line shows the σ_c of pure cement. These plots are grouped from left to right by concentration, and are organized within each group by particle size (smallest to largest in each group). Comparing the raw ulva results, we see that biomass concentration is inversely proprtional to σ_c in a nonlinear manner at each particle size. This drop in mechanical performance is expected as previous work has seen similar results where there is a low-strength plateau at 5% [43], though this was with spirulina microalgae rather than the ulva macroalgae here. Compared to this dramatic decrease in mechcanical performance with microalgae filler, the raw ulva macroalgae seems to

perform similarly both at 1% and 5% before experiencing a drop at 10%. Looking at the self-bonded ulva results (**Figure 6b**), there is a similar trend, though the decrease in performance at 10% is less dramatic. This indicates that the effect of self-bonding biomass creates a strength enhancement, and therefore an opportunity for higher amounts of cement replacement, but this will be discussed in further detail in this section. Regarding the effect of concentration, we can see that an increase in concentration will decrease the steady-state σ_c of the macroalgae-cement composites a significant amount at 10%. It is also important to note than when considering the effects of both particle size and self-bonding, higher concentrations will enhance their effect as higher amounts of the composite filler will be present in the final sample.

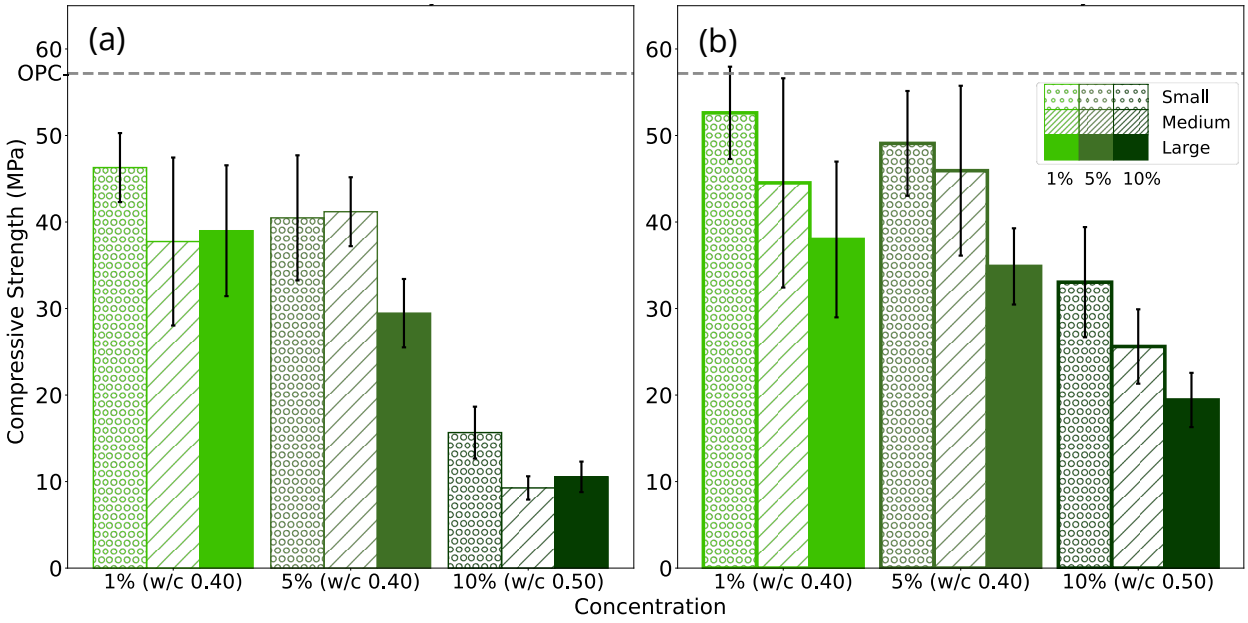

Figure 6. Steady-state ultimate compressive strength of 1%, 5%, and 10% ulva at small (dotted), medium (dashed) and large (solid) particle sizes both in (a) raw and (b) self-bonded forms.

Looking at each individual group of bar plots in **Figure 6**, we can then observe the effect of particle size at each concentration for raw and self-bonded materials. Considering the variance of the samples, we see no significant effect of particle size on the mechancial

performance of the 1% macroalgae-cement composites at steady-state. However, at 5 and 10% for both the raw and self-bonded samples, the largest particle size is significantly weaker at steady-state than the smallest particle size while the medium particle is inconsistent with its behavior relative to the small and large sizes. Similar trends in particle size for both raw and self-bonded results suggests that self-bonding does not change the effect of particle size.

Considering the effect of self-bonding, we can compare the grouped concentration plots in **Figure 6a** with the same respective concentrations in **Figure 6b** (comparing 1% raw with 1% self-bonded, etc.). Similar to the trend observed with the effect of particle size, there is no observable significant difference when comparing the 1% raw and self-bonded samples. Once again, a trend becomes observable at 5 and 10%; self-bonded biomass enhances the steady-state σ_c by as much as 21.26% and 176.39% respectivley compared to raw biomass at the same particle size. This imporovement is especially significant for samples containing 10% self-bonded ulva where small, medium, and large particle size samples experience a respective increase of 17.38, 16.35, and 8.89 MPa in their average σ_c. At 5%, the enhancements are a less dramatic 8.60 (small), 4.74 (medium), and 5.4 (large) MPa. These results indicate that self-bonding ulva as a preprocessing step for cement additions leads to an increase in mechanical properties relative to utilizing raw biomass. This observed enhancement is more significant as particle size decreases and is best represented at 10% where the filler concentration (and therefore the amount of self-bonded particles) is highest. Both of these factors increase the surface area of self-bonded particles, meaning this could be an explanation for the strength enhancement becoming

more dramatic. While discussing this enhancement as a result of particle size and self-bonding, it is important to note that the overall mechancial performance significantly decreases when the concentration of ulva is increased from 5% to 10%. However, all self-bonded ulva samples other than the largest particle 10% sample meet the 21 MPa requiment for light commercial and residential applications [12]. More impressively, the 5% self-bonded ulva of the smallest particle size even meets the 41 MPa strength requirements for structural applications [13], highlighting the opportunity for using self-bonded ulva to reduce the carbon footprint of cement.

The strength development curves of the samples are compared in **Figure 7**. We utilize **Equation 6** proposed by Lin et al. [43] to evaluate the strength evolution, where σ_f is the plateau strength and τ is the characteristic curing time (days) for that sample to reach a plateau in strength.

$$\sigma(t) = \sigma_f \left(1 - e^{-t/\tau}\right) \quad (6)$$

Comparing the effect of concentration in **Figure 7a-c**, we cannot confidently discern a pattern between 1% and 5% raw ulva strength curves with characteristic τ values within 0.3 days of one another at the two larger particle sizes (**Figure 7b-c**). At the smallest particle size (**Figure 7a**), there is a more noticeable difference of 1.8 days. We observe a significant retardation in the 10% samples compared to 1% and 5% at all particle sizes, as the τ value increases from 3.83 days in the 1% samples to 11.57 days for the 10% sample. This result agrees with the steady-state mechanical results in **Figure 6** where raw ulva samples at 1% and 5% are comparable before a significant drop in performance at 10%.

The τ values are all statistically similar when observing the effect of particle size and self-bonding. The strength devleopment curves comparing self-bonding do show that self-bonding biomass enhances the strength devleopment. Furhtermore, this effect is more apparent as strength increases.

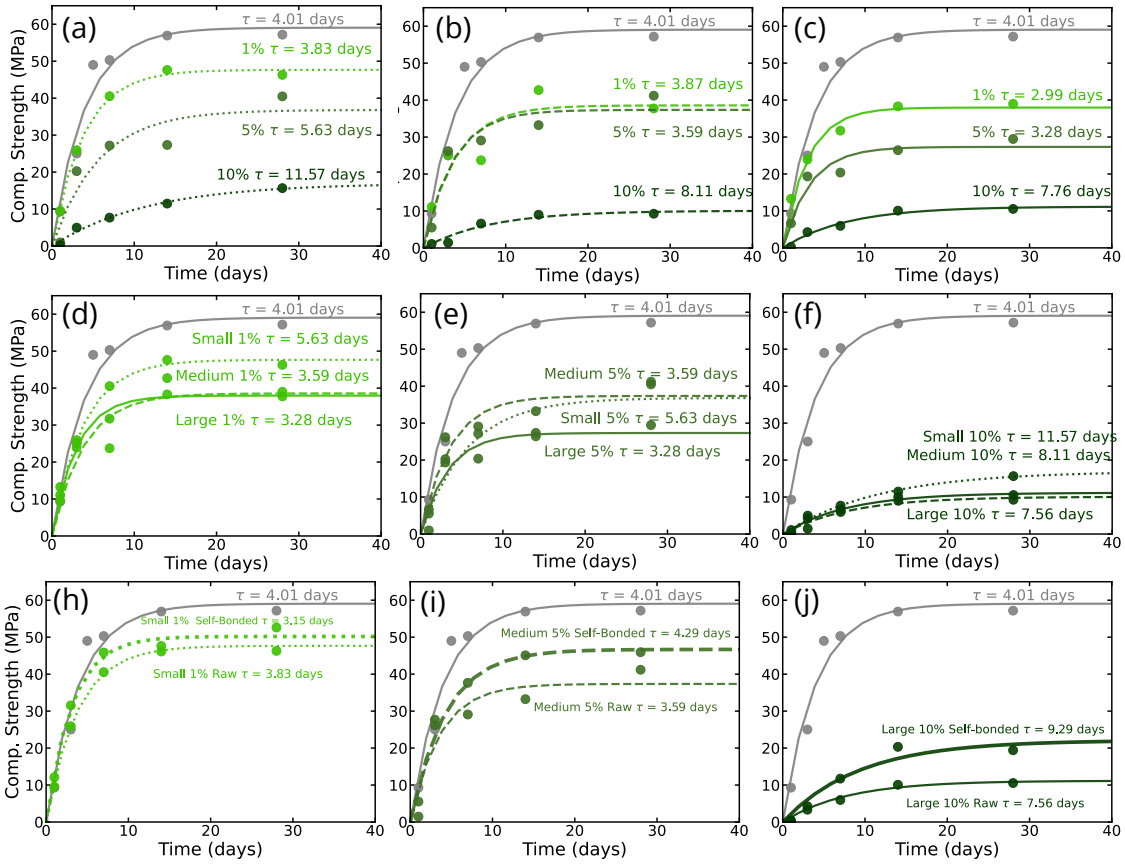

Figure 7. Strength development curves of ulva-cement composites. The first row presents the curves of raw ulva at (a) small, (b) medium, and (c) large particle sizes in order to compare the effect of concentration. The second row presents the curves of raw ulva at (d) 1%, (e) 5%, and (f) 10% to compare the effect of particle size. The third row presents the curves of raw and self-bonded ulva at (h) small particle size 1% concentration, (i) medium particle size 5% concentration, and (j) large particle size 10% concentration to see the effect of self-bonding.

3.1.2 Effect on hydration reactions

Pure cement and the biomass composites were analyzed via TGA to observe any differences in the steady-state hydration products. TGA data was normalized to 140 °C to negate the loss of water entrapped in pores. **Figure 8** presents the TGA curves for various ulva-cement composites. As mentioned in *Section 2.7*, the initial portion of the TGA curves is to eliminate any water loss which may be attributed to water entrapped in pores, as well as uptake accounted for by the biomass. It is noted that particle size and self-bonding may

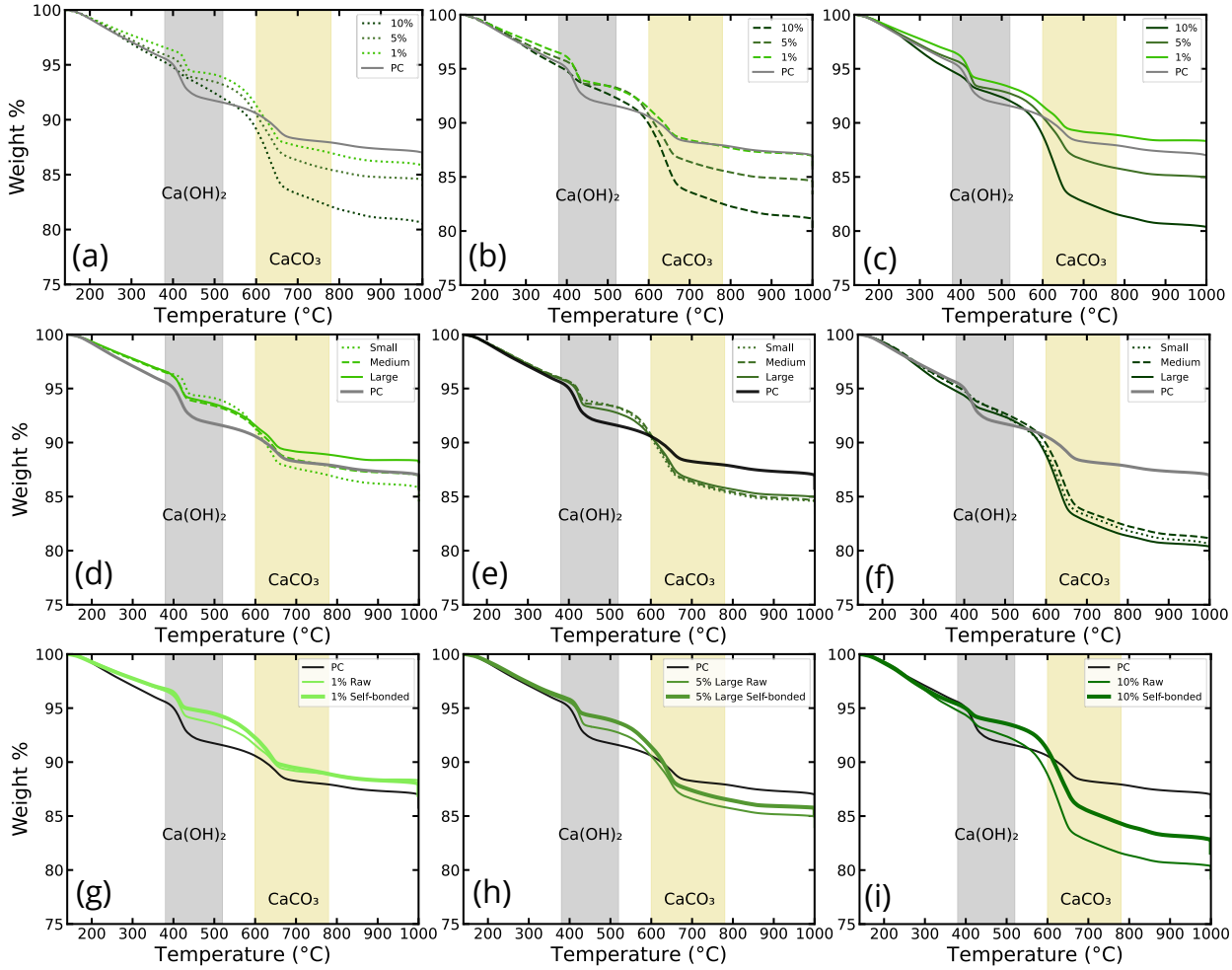

Figure 8. Thermal degradation of ulva-cement composites. The first row presents the curves for raw ulva at (a) small, (b) medium, and (c) large particle sizes to observe the effect of concentration. The second row groups raw ulva composites by (d) 1%, (e) 5%, and (f) 10% to observe the effect of particle size. The third row presents compares the raw and self-bonded ulva composites at (g) 1%, (h) 5%, and (i) 10%, all at the largest particle size.

influence the water uptake of the algae, though that has not been directly compared in this study. There are two shaded regions in the TGA curves; the grey region spans from 380 °C to 520 °C and is attributed to the decomposition of $Ca(OH)_2$, while the yellow region spans from 600 °C to 780 °C and is related to a decomposition of $CaCO_3$ [54], [55]. There is mass loss occuring over the entire temperature regiment which can be attributed to the decomposition of the amorpohus C-S-H [54]–[56] as well as the algal biomatter [57]. These mechanisms for thermal degradation are considered when observing the effects of the concentration, particle size, and self-bonding as an indicator for the hydration reactions derived from alite and belite (**Equations 2 and 3**).

The pure cement degradation profile is visually discernable in behavior from the composite curves, and the composites themselves show a correlation with concentration. By calculating the area of the derivative curve of the TGA within the $Ca(OH)_2$ decomposition region we find that the pure cement sample contains approximately 3.5% $Ca(OH)_2$ while the 1% and 5% small particle size composites contain approxiamtely 1% and the 10% composite does not appear to present this characteristic decomposition (**Figure 8a**). This trend in concentration is observed regardless of particle size for the raw ulva composites (**Figure 8b-c**). The difference in degradation profiles suggests that adding up to 5% of raw ulva will partially hinder the primary hydration reactions that occur in pure cement while not entirely halting them, but reaching a concentration of 10% amplifies this effect drastically. The 10% sample differing from the 1% and 5% in this manner could be reflected by a decrease in steady-state mechanical performance, which is what we observe in both raw and self-bonded ulva when comparing concentration solely. The mass loss falling in

the $CaCO_3$ region becomes more dramatic with increasing concentration and may be related to the ulva degradation [57], but there is no method utilized in this experiment to conclusively deconvolute the contributions from this, $CaCO_3$, C-S-H, and other carbonated phases [54] solely through TGA.

Overall, the effect of particle size appears to be fairly minimal at all concentrations. At 5% and 10%, the raw ulva composites of all particle sizes present nearly identical degradation (**Figure 8e** and **8f**, respectively). **Figure 8d** indicates that for the 1% samples, there are some slight devations at the tail end (> 800 °C), but there is nothing significant enough to warrant further investigation. Most importantly, all peaks of the same concentration observe similar behavior in the $Ca(OH)_2$ region, suggesting that particle size plays a small role towards the effect on hydration reactions. This again aligns with the mechanical results of raw ulva at steady-state, as there is no significant difference in the σ_c of different particle sizes of filler at similar concentrations.

The degradation profiles are once again reorganized to analyze the effect of self-bonding on the composites in **Figure 8g-i**. While the profiles appear overall very similar, the self-bonded samples undergo a smaller mass loss in the $Ca(OH)_2$ region. These differences in mass loss are insignificant towards the overall hydration reactions. There is less mass loss in self-bonded algae composites compared to raw counterparts, and this is more observable as concentration increases. There is a possibility that the self-bonded particles have reinforced thermal stability, though this cannot be confirmed through this experiment and is unlikely to carry an impact to the mechanical strength. Therefore, the root cause of the strength enhancement from self-bonding is not a chemical source.

3.1.3 Effect on micromorphology

To further investigate the interactions between the cement matrix and the algae fillers, SEM analysis was conducted after both 7 and 28 days of composite curing. The interface between the filler and the matrix are of the most importance during this analysis; as explained in the introduction, a stronger interface between the biomass and cement matrix will prevent defect driven fracture.

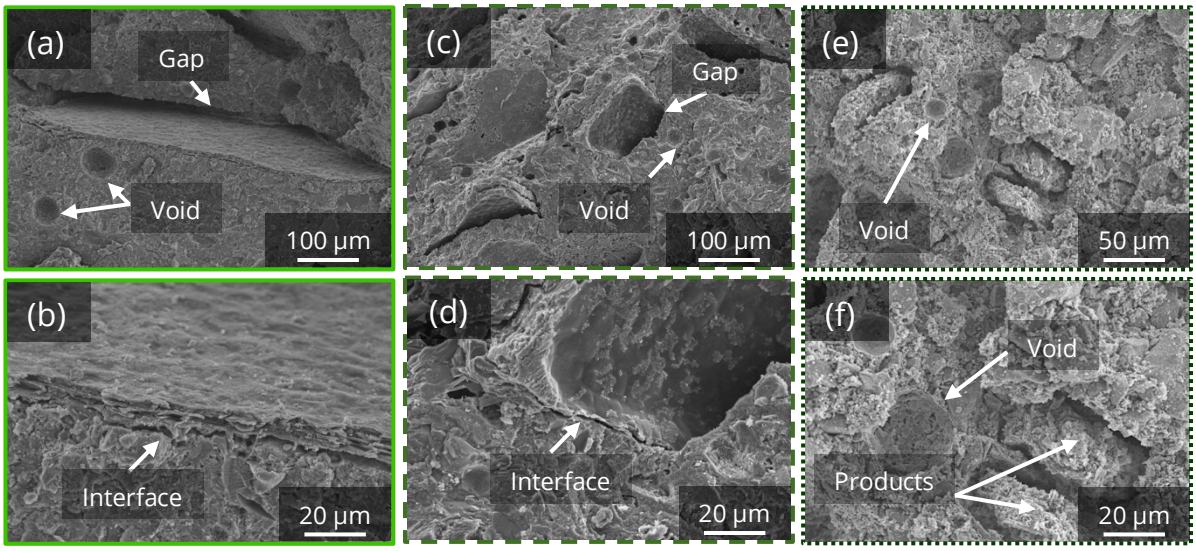

Figure 9. Steady state micromorphology. SEM images of (a-b) large, (c-d) medium, and (e-f) small raw ulva particles in cement composites with concentrations of 1%, 5%, and 10% respectively.

The mechanical results and degradation profiles suggest the effect of particle size is expected to be similar at each concentration, so there is no SEM analysis explored to explicitly expand on these observations. First looking at the effect of concentration, the cement matrix appears to become less densified with increasing concentration and the presence of voids increases. Although there appears to be more voids (10-30 µm) in the 10% (**Figure 9e-f**) and 5% (**Figure 9c-d**) samples compared to the 1% (**Figure 9a-b**) samples, SEM analysis is not a quantitative method to holistically classify this trend. These

are both potential sources for the decreasing mechanical performance of the composites with increasing concentration; a less densified cement matrix is indicative of hindered hydration, and the increased presence of voids adds more defects to the composite which may lead to earlier fracture. As mentioned before, the thermal degradation results agree with the observation that hydration reactions are less fulfilled when adding higher concentrations of biomass. The increased filler concentration will certainly play a role in the strength, and more quantitative methods to discern the more dominant mechanism in terms of interface interactions and fracture mechanics are recommended beyond this experiment.

Regarding the effect of particle size, the two larger particle sizes share similarities in their filler-matrix interfaces. Ulva biomass used in this experiment takes a flake-like structure; the flake surface in both the large and medium particles seem to have no interaction with the cement matrix. In fact, there is a very noticeable gap that forms between the matrix and flake surface, as shown in **Figure 9a** and **9c** Additionally, the interface between the matrix and filler is very distinct, highlighted in Figure **9b** and **9d**. The small particles differ in micromorphology, as there appears to be some product growing on the surface of the filler particles, highlighted in **Figure 9f**. Despite the products observed, there is still a clear gap between the matrix and filler as in the larger two particle sizes. Regardless of the differing interactions with the cement matrix depending on particle size, the mechanical and degradation results indicate no significant effect on the mechanical performance and hydration products formed. Therefore, the dominant effect appears to be concentration rather than particle size for the raw ulva.

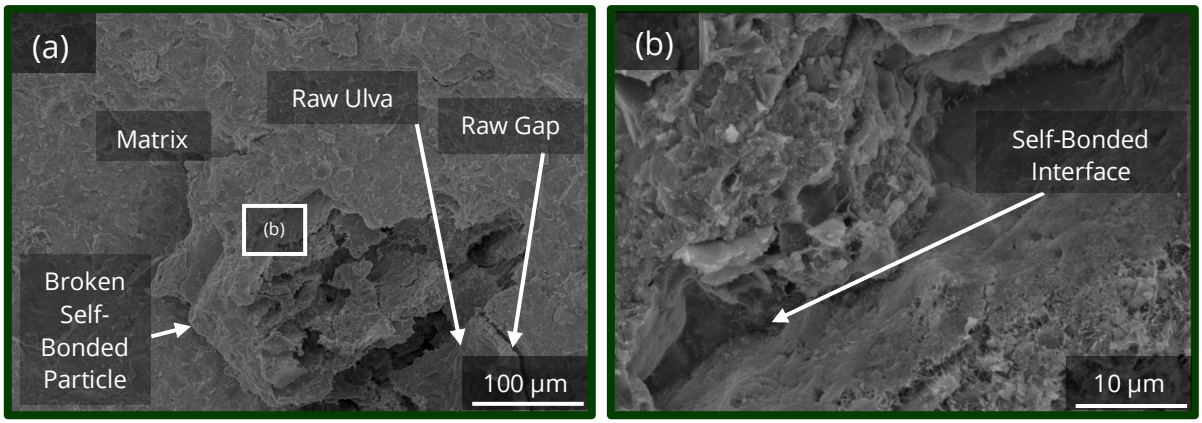

Figure 10. Steady-state micromorphology to observe self-bonded ulva. Self-bonded ulva at large particle size in cement composites with 10% concentration. (a) Low magnification image to see the whole particle in the matrix and (b) high magnification image to closely observe the interface between the self-bonded particle and cement matrix.

Now discussing the effect of self-bonding, **Figure 10** show a large self-bonded ulva particle in a 10% concentration sample at steady state. This image reveals information regarding both the degree of self-bonding as well as its effectiveness as a filler relative to raw ulva. Looking at the degree of self-bonding, **Figure 10a** shows a cluster of raw ulva that was previously encapsulated by an outer layer which can be interpreted as self-bonded ulva; this suggests that the hot pressing does not self-bond every particle of ulva. **Figure 10a** also points out a raw ulva particle, which still has visible cells and an easily observed gap between the biomass and cement matrix. Now looking at **Figure 10b**, we observe a much more developed interface between the self-bonded ulva and the cement matrix. Considering the effect of interfacial strength on composite performance [24]–[26], these micromorphology observations agree with the mechanical results where a strength enhancement is observed as an effect of using self-bonded additives. Therefore, the strength enhancement seen in self-bonded biomass results from stronger interface developments between the biomass and the cement matrix serving as increased

mechanical reinforcement. Furthermore, the mechanical results also depicted this enhancement becoming stronger as particle size decreases. These observations explain the strengthening observed in self-bonded composites despite the degradation profiles suggesting a less fulfilled hydration. However, again regarding the degree of self-bonding, the presence of raw ulva indicates that self-bonding can be further optimized such that a higher percentage of the raw biomass processed is receives the intended treatment.

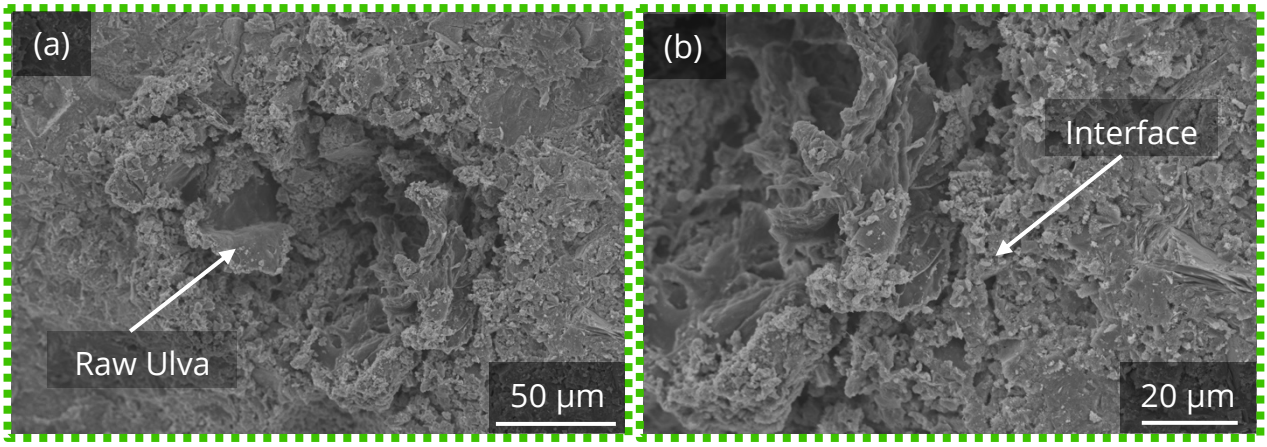

Figure 11. Steady-state micromorphology to observe self-bonded ulva. Self-bonded ulva at small particle size in cement composites with 1% concentration. (a) Low magnification image to see the whole particle in the matrix and (b) high magnification image to closely observe the interface between the self-bonded particle and cement matrix.

Figure 11 above again looks at the effect of self-bonding, but at the small particle size. Similar to with what is seen in **Figure 10a**, **Figure 11a** points out a raw ulva particle within what appears to be a self-bonded cluster. The higher magnification image presented in **Figure 11b** shows an interface seemingly less dense than the interface in **Figure 10b**, but with no clear gap or interface seen in all the raw ulva composites shown in **Figure 9**. This observation suggests that the interface microstructure between ulva and cement are influenced by the compounding effects of particle size and self-bonding pretreatment, yet the self-bonding pretreatment is more effective in creating a dense interface.

Combining the results from the compression testing and micromorphology, we propose a hypothesis to explain the significant strength enhancement in composites containing small and self-bonded ulva. As mentioned in the *Section 2.3*, the self-bonded particles were grinded down and further processed to achieve different particle size ranges. In the case of the smaller particles, speed-milling was the method of choice. If the observations from **Figure 10** are true, it is then expected that smaller particle size ranges would break up these clusters of ulva particles with self-bonded boundaries and raw ulva within. The mechanical results indicate that self-bonding strengthens the composites, which becomes more effective as particle size decreases. Therefore, a viable explanation for this strength enhancement is explained by the increased surface area of self-bonded ulva as particle size decreases. As the surface area of self-bonded ulva increases, there will be an increased number of strengthened interfaces with the cement matrix relative to its raw counterpart. Therefore, more strong interfaces will result in stronger composite performance. No sample in this work exceeds the experimental or literature σ_c of pure cement; however, this could potentially be achieved if the efficiency of the self-bonding process is optimized to subsequently increase the overall interfacial strength. The observations explored in this section are noted, as they will later be compared with the observed effects of spirulina microalgae in the following section.

3.2 Effects of spirulina microalgae on cement composites

As a comparison to the macroalgae, we now look at the effect of microalgae on the cement composites. Again, each characterization method is isolated for discussion: mechanical

results, followed by thermal degradation profiles, and micromorphological assessments. Finally, we then compare the microalgae results with the macroalgae results.

3.2.1 Mechanical Results

The steady-state mechanical performance is considered in below where **Figure 12a** shows the 28-day σ_c of raw spirulina cement composites and **Figure 12b** shows such for self-bonded cement composites. The black dashed line again shows the σ_c of pure cement. These plots are grouped from left to right by concentration, and are organized within each group by particle size (smallest to largest in each group). Also note that only the small particle size is explored for raw spirulina, as this was the out-of-bag condition. The same trend is present with concentration for both the self-bonded and raw results, where we see a significant drop in strength when biomass concentration reaches 5%. This agrees with previous work where spirulina concentration created a plateau in strength drop off at 5% [43], where it was discovered that this strength decrease was largely due to the retardation of hydration reactions. Looking at the self-bonded results, the self-bonded spirulina with 1% concentration is significantly weaker than the raw filler. Contrary to the strength enhancement seen in macroalgae, self-bonding pretreatment appears to further hinder the mechanical performance of the microalgae composites.

Looking at each individual group of bar plots in **Figure 12b**, we can then observe the effect of particle size at each concentration for self-bonded materials. The largest particle size samples for 1% and 5% concentration appear to be weaker than the two smaller particle sizes, with the difference being larger in the 1% sample. However, at 10% for the

self-bonded samples, there is no apparent effect of particle size. This is drastically different from the macroalgae results where the effect of particle size and self-bonding is more observable as concentration increases. This suggests that the retardation effect from spirulina concentration is more dominant than the effects of particle size or self-bonding.

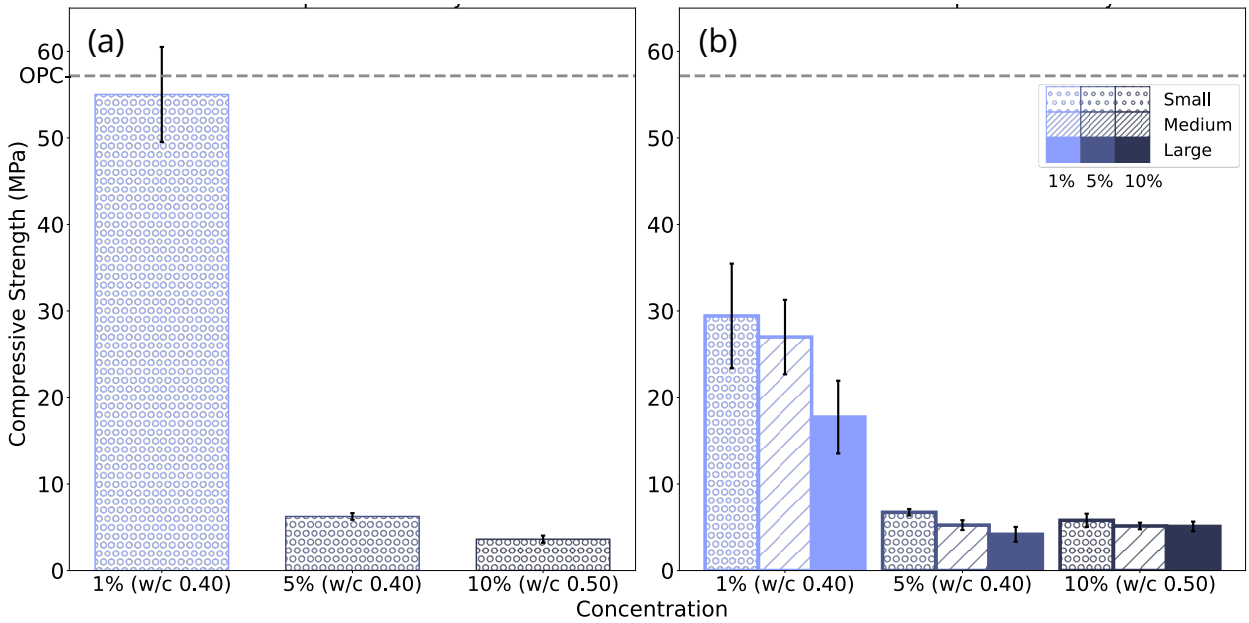

Figure 12. Steady-state ultimate compressive strength of 1%, 5%, and 10% spirulina at small (dotted), medium (dashed) and large (solid) particle sizes both in (a) raw and (b) self-bonded forms. Note again that (a) raw spirulina was only tested at the small particle size.

As mentioned, the effect of concentration appears to be dominant over both the particle size and self-bonding mechanisms here. This is supported by the 5% and 10% self-bonded samples showing nearly identical steady-state σ_c (6.25 MPa and 3.62 MPa respectivley) to the raw counterparts (6.73 MPa and 5.80 MPa). Though both values get lower, it is still clear that self-bonding does not create the intended enhancement. At 1%, the raw steady-state σ_c decreases from 55.02 MPa to 29.42 MPa as a result of self-bonding. The reason for this dramatic decrease in strength is considered in the next sections.

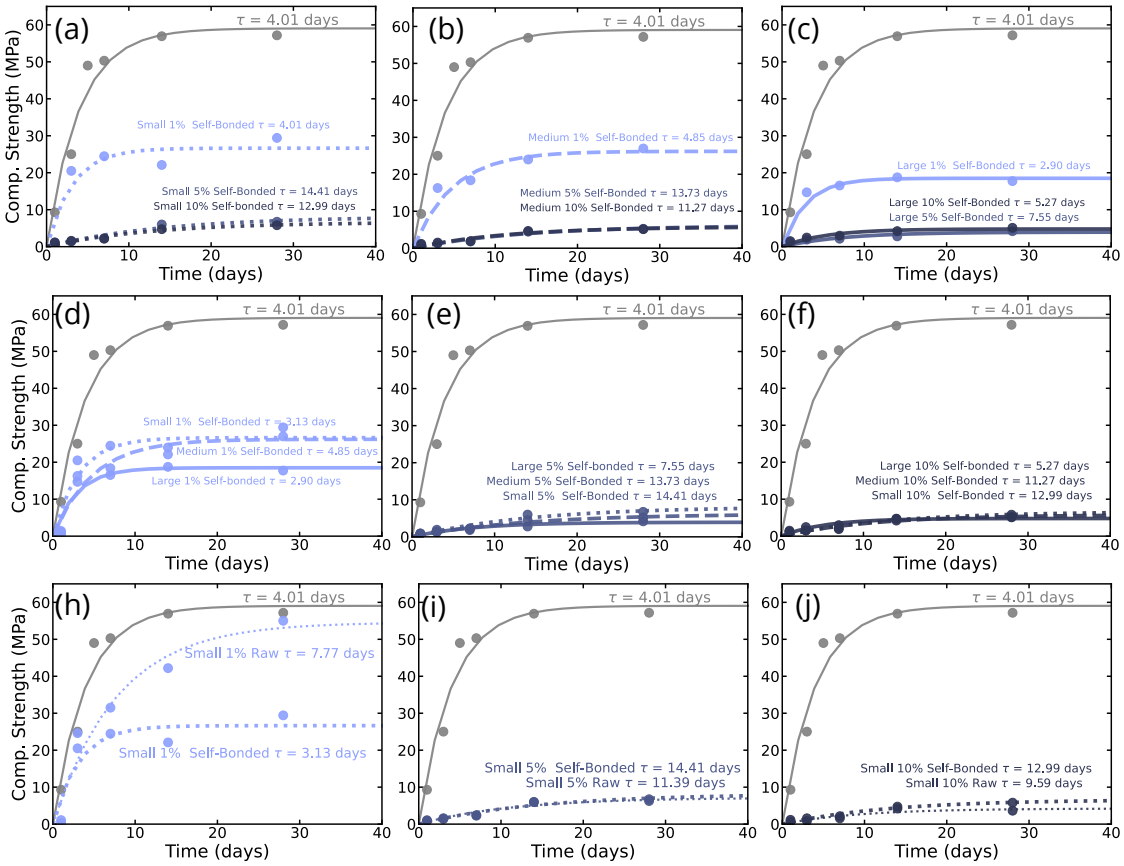

Figure 13. Strength development curves of spirulina-cement composites. The first row presents the curves of self-bonded spirulina at (a) small, (b) medium, and (c) large particle sizes in order to compare the effect of concentration. The second row presents the curves of self-bonded spirulina at (d) 1%, (e) 5%, and (f) 10% to compare the effect of particle size. The third row presents the curves of raw and self-bonded spirulina at (h) 1%, (i) 5%, and (j) 10% concentration to see the effect of self-bonding, all at small particle size.

The strength development curves of the spirulina samples are compared in **Figure 13**. Looking first at the effect of conentration, we see that small and medium (**Figure 13a-b**, respectively) particle sizes cause a significant retardation in the strength development at and above 5% concentration. Comparing 1% and 5%, the characteristic τ value increases by 10.4 days and 8.88 days at small and medium particle sizes, respectively. Yet, less retardation difference is observed for large particles when increasing concentration from 1 to 5%. Moreover, despite the curves looking similar between particle sizes for a given concentration (**Figure 12d-f**), the characteristic τ values indicate a dramatic retardation

when small and medium particles are utilized. This is most prevalent at 5% and 10% where more biomass is present in the composite; here, the τ value increases by 6.18 and 6.00 at 5% and 10% respectively as particle size changes from large to medium. Now looking at the effect of self-bonding, we see similar trends to what was observed in the steady-state σ_c. Although there is no significant trend on the characteristic τ, we see the strength development plateau at a lower compressive strength in the 1% self-bonded sample compared to the raw sample. This trend is no longer present at and above 5%, agreeing with the expected plateau [43].

3.1.2 Effect on hydration reactions

Figure 14 presents the steady-state TGA curves for 1%, 5%, and 10% spirulina composites in the raw form at small particle size range (**Figure 14a**), self-bonded at the small particle size range (**Figure 14b**), and self-bonded at the large (**Figure 14c**) particle size range. The pure cement sample contains approximately 3.5% $Ca(OH)_2$ while the 1% raw composites contain approxiamtely 2.5%. Yet, the 5% and 10% composite do not present this characteristic decomposition which agrees with the steady-state compressive strength where a dramatic decrease at and above 5% concentration is seen. Therefore, we note that the hindrance of the cement hydration reactions are likely a contributor to the poor σ_c of the spirulina composites at 5% and 10% concentration.

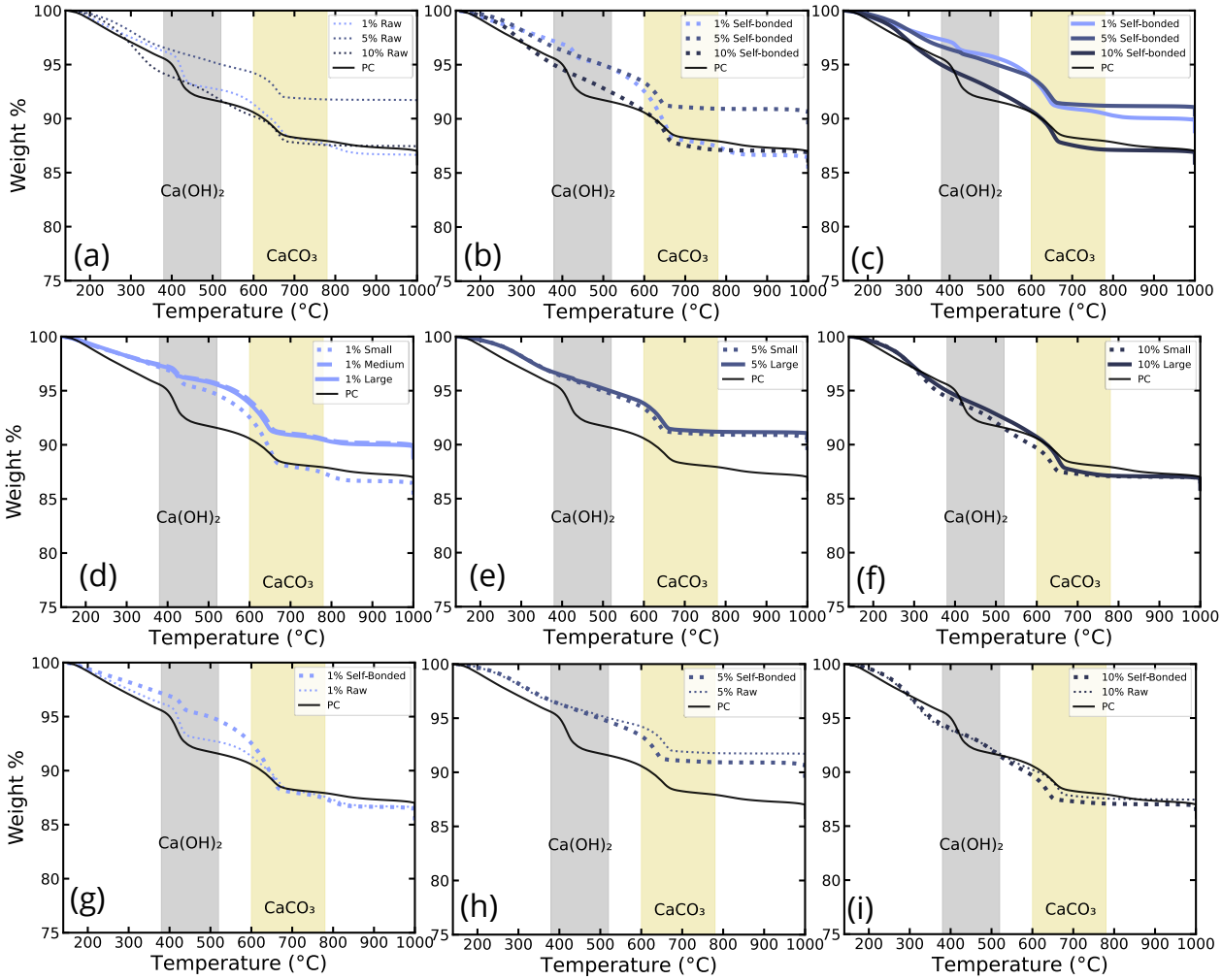

Figure 14. Thermal degradation of spirulina-cement composites. The first row presents the curves for self-bonded spirulina at (a) small, (b) medium, and (c) large particle sizes to observe the effect of concentration. The second row groups self-bonded spirulina composites by (d) 1%, (e) 5%, and (f) 10% to observe the effect of particle size. The third row presents compares the raw and self-bonded spirulina composites at (g) 1%, (h) 5%, and (i) 10%, all at the smallest particle size.

Overall, the effect of particle size (**Figure 14d-f**) appears to be fairly minimal at all concentrations. Again, all peaks of the same concentration observe similar behavior in the $Ca(OH)_2$ region, suggesting that particle size plays a smaller role here similar to in raw ulva; this finding is again in agreement with the mechanical results. Most notably, the smallest particle size of the 1% (**Figure 14d**) composites undergoes more degradatoin above 500 °C; this trend is not present in the 5% (**Figure 14e**) and 10% (**Figure 14f**) samples, which can be

investigated further. Regarding the effect of self-bonding at 1%, the profile shows a smaller mass loss in the $Ca(OH)_2$ region for the self-bonded spirulina composites compared to the raw powder spirulina, explaining the decreased compressive strength with self-bonding pretreatment previously observed. This differing profile aligns with the observed compressive strength, suggesting that self-bonding further retards the hydration reactions and strength development relative to the raw powder. This trend is not observed at either 5% (**Figure 14h**) or 10% (**Figure 14i**), which again suggests that the effect of concentration is a more influential factor on the hydration reactions and mechanical performance than the effect of self-bonding.

3.1.3 Effect on micromorphology

Figure 15 presents SEM images taken at day 7 of 10% spirulina concentration as a raw filler (**Figure 15a-b**), a self-bonded filler (**Figure 15c-d**), and a self-bonded filler with large particle size (**Figure 15e-f**). Here, the 10% 7-day samples are presented due to difficulties observing the particle-matrix interface at lower concentrations and at steady-state. It is noted that the interface is not expected to change with varying concentration, and the interactions between the filler and matrix can still be compared at day 7.

The micromorphology of the 10% raw spirulina (**Figure 15a-b**) align with the observations from previous work imaging microalgae filler [43], where we see nanofibers (~ 500 nm) at the cement-biomass interface that have a different morphology than typical hydration products and may therefore not be the amorphous C-S-H which strengthens

cement. There is also a noticeable gap between the spirulina and the matrix, which could be caused by the water lost by the biomass as it dehydrates and subsequently shrinks.

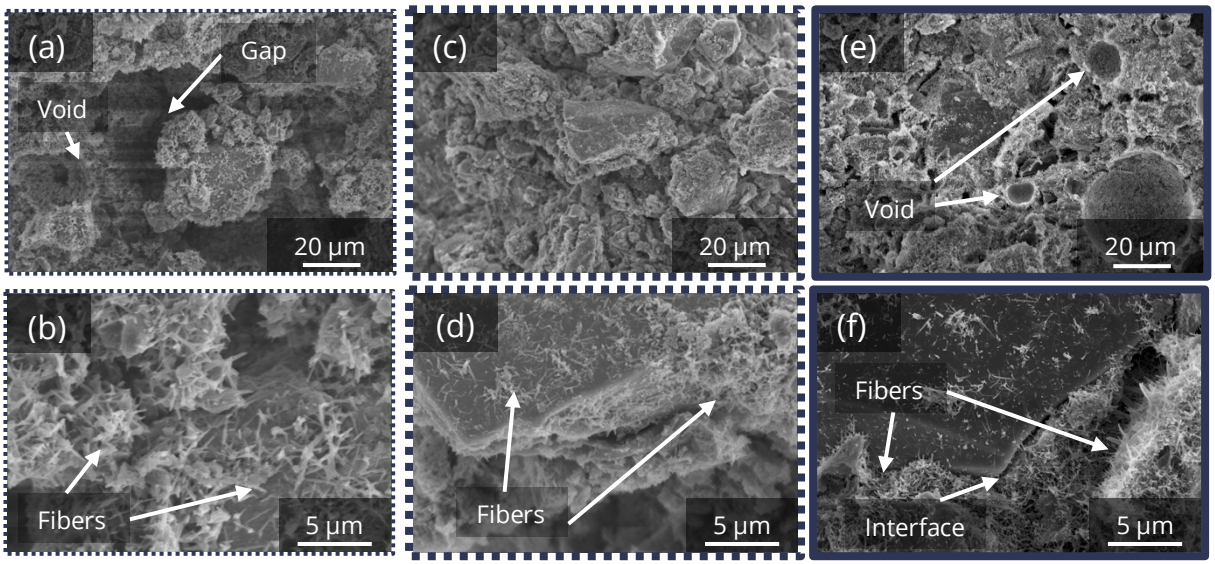

Figure 15. Early-stage micromorphology to observe self-bonded ulva and the interface. SEM images of (a-b) small particle size raw spirulina, (c-d) small particle size self-bonded spirulina, and (e-f) large particle size self-bonded spirulina in cement composites. All imaged samples are 10% concentration.

Now comparing the composites with raw spirulina (**Figure 15a-b**) and the self-bonded spirulina (**Figure 15c-d**), the first similarity is the presence of the same fibers at higher magnification, though less significantly in the self-bonded biomass. The very distinct gap between the matrix and spirulina in the raw powder is much less pronounced in the self-bonded sample. This is an indication that the self-bonding may play a role in affecting the interactions between the cement matrix and the biomass, but this cannot be explored further through SEM analysis. Regardless, self-bonding has no significant impact on steady-state strength at 5% or 10%, and even weakens the composite at 1%. This result almost exactly contradicts what is seen with the ulva results, warranting further discussion and exploration.

Regarding the effect of particle size, the small (**Figure 15c-d**) and large (**Figure 15e-f**) particle sizes of self-bonded spirulina look nearly identical, as expected. The large particle composite again has comparatively few fibers on the biomass surface, with many of these products at the interface with the cement matrix. There are also voids ranging from 5-30 μm observed. Nonetheless, the similar degradation and mechanical performance indicates that there is no significant effect of particle size on the hydration reactions and strength, which is also seen here.

Now comparing the microalgae and macroalgae, we observe differences in their behavior arising from self-bonding. In short, we see that spirulina influences on cement composite strength is rooted in the chemical interactions sufficiently retarding the hydration reactions; conversely, the ulva appears to have comparatively little impact on the hydration reactions and the effects on cement composite strength are governed by the mechanical reinforcement the ulva filler provides. Compositionally, macroalgae can have a protein content ranging from 7-31% of the dry weight, lipid content in the 2-13% range, a carbohydrate content of 32-60% [58], [59], and cellulose contents from 1-15% [60]. Conversely, microalgae is rich in carbohydrates, proteins and lipids [61]. The main differences between the macroalgae and microalgae is the significant amount of cellulose in the multicellular macroalgae structure, and the protein rich environment of the unicellular microalgae. It is expected that the self-bonding of spirulina exposes more proteins and cellular innards, which carries the detrimental influence on the compressive strength. It is therefore hypothesized that similar interactions from ulva self-bonding have an strengthening effect, though this is an area to explore in further experimentation.

Conclusion

In this work, macroalgae in the form of ulva and microalgae in the form of commercial spirulina underwent preprocessing to alter the particle size as well as to self-bond the biomass. Resultant composites were characterized by their mechanical strength and strength development over 28 days of curing, thermal degradation studies at steady-state, and micromorphological assessments at both early (7 day) and late (28 day) stages of curing. The results gathered support the following general conclusions:

- We observed a decrease in compressive strength with increasing concentration of raw ulva at and above 10%, where the addition of 1 and 5% raw ulva have similar effects on cement composites in terms of their mechanical performance, hydration products and micromorphology. The small particle ulva (25 +/- 19.7 um) composites are ~1.5x stronger than the large particle (272.1 +/- 124.9 um) counterparts. In addition, we found that the particle sizes of raw ulva have negligible effect on the hydration reactions due to the similar TGA degradation profile. While a gap between the biomass and the matrix is observed in SEM analysis for all raw ulva, the effect of particle size is best explained by defect mechanisms where smaller defects will hinder the strength less. Leveraging the self-bonding preprocessing, we show the potential of enhancing the compressive strength of ulva-cement composite up to 2-fold (from 15.66 MPa to 33.04 MPa) at 10% small particle ulva concentration. This strength enhancement is attributed to the reduced gap at the filler-matrix interfaces seen in the micromorphology, which may be caused by the change

in hydrophilicity of biomass through the self-bonding preprocessing; this change will lead to stronger interfacial bonding, as well as intrinsically stronger additives. Highlighting the improved interfacial bonding through self-bonding preprocessing, increasing filler surface area (decreasing particle size) also shows an increase in compressive strength.

- In contrast to the macroalgae, spirulina shows a concentration-dominated mechanism where more than 5% addition of raw or self-bonded spirulina drastically hinders both the cement hydration reactions and the mechanical performance. Surprisingly, when 1% self-bonded spirulina is introduced, the compressive strength of the composite decreases by a factor of 0.53 compared to the raw spirulina counterparts. We hypothesize that this reduction in strength is induced by the self-bonding processing that enhances the detrimental chemical interactions between the spirulina filler and the cement matrix. The contrary effect of self-bonded bio-additives on cement between ulva and spirulina is attributed to the compositional differences between the macro and micro-algal species, which is beyond the scope of this work.

Future work can optimize the current experiments as well as further characterize what is observed. For example, future work can utilize a singular method of particle size processing that narrows the ranges further and optimize self-bonding pretreatment to increase the degree of self-bonding in biomass. aim to narrow particle size better. Further work can characterize these composites to develop stronger understandings of the observed mechanisms. This work identified that the biomass surface area in cement composites is likely the driving mechanism for the mechanical performance. Therefore, future experiments can aim to deconvolute the effects seen in this work by treating

surface area as the independent variable. The surface area of biomass particles can be found using techniques such as mercury intrusion porosimetry and the Brunauer-Emmett-Teller (BET) method [62]–[65]. The self-bonding pretreatment can be understood by a) finding the strength values of self-bonded ulva, b) utilizing methods such as the sessile drop measurement to compare contact angles and hydrophilicities between biomasses, c) studying what chemical differences arise from self-bonded biomass through X-ray photoelectron spectroscopy, and d) quantifying the interfacial strength through nanoindentation probing the interface in these composites.

References

[1] S. H. Kosmatka and M. L. Wilson, “Design and Control of Concrete Mixtures,” *Portland Cem. Assoc.*, vol. Fifteenth Edition, p. 459, 2011.

[2] Keegan Ramsden, “Cement and Concrete: The Environmental Impact,” Nov. 03, 2020. https://psci.princeton.edu/tips/2020/11/3/cement-and-concrete-the-environmental-impact

[3] A. Talaei, D. Pier, A. V. Iyer, M. Ahiduzzaman, and A. Kumar, “Assessment of long-term energy efficiency improvement and greenhouse gas emissions mitigation options for the cement industry,” *Energy*, vol. 170, pp. 1051–1066, Mar. 2019, doi: 10.1016/j.energy.2018.12.088.

[4] R. Kajaste and M. Hurme, “Cement industry greenhouse gas emissions – management options and abatement cost,” *J. Clean. Prod.*, vol. 112, pp. 4041–4052, Jan. 2016, doi: 10.1016/j.jclepro.2015.07.055.

[5] S. Balsara, P. K. Jain, and A. Ramesh, “An integrated approach using AHP and DEMATEL for evaluating climate change mitigation strategies of the Indian cement manufacturing industry,” *Environ. Pollut.*, vol. 252, pp. 863–878, Sep. 2019, doi: 10.1016/j.envpol.2019.05.059.

[6] A. Hasanbeigi, L. Price, and E. Lin, “Emerging energy-efficiency and CO2 emission-reduction technologies for cement and concrete production: A technical review,” *Renew. Sustain. Energy Rev.*, vol. 16, no. 8, pp. 6220–6238, Oct. 2012, doi: 10.1016/j.rser.2012.07.019.

[7] “Carbon Foot Print.indd,” p. 2.

[8] E. Gartner, “Industrially interesting approaches to ‘low-CO2’ cements,” *Cem. Concr. Res.*, vol. 34, no. 9, pp. 1489–1498, Sep. 2004, doi: 10.1016/j.cemconres.2004.01.021.

[9] Robert Courland, *Concrete planet : the strange and fascinating story of the world’s most common man-made material.* Amherst, N.Y.: Prometheus Books.

[10] M. Soustos and P. Domone, *Construction Materials: Their Nature and Behaviour*, 5th ed. CRC Press, 2017. [Online]. Available: https://doi.org/10.1201/9781315164595

[11] Y. Xu and D. D. L. Chung, “Improving silica fume cement by using silane,” *Cem. Concr. Res.*, vol. 30, no. 8, pp. 1305–1311, Aug. 2000, doi: 10.1016/S0008-8846(00)00337-9.

[12] K. H. Obla, R. L. Hill, and R. S. Martin, “HV.A Concrete An Industry Perspective”.

[13] Gerald B. Neville, P.E., “The Strength of Concrete,” in *Concrete Manual 2012 IBC and ACI 318-II Concrete Quality and Field Practices*, ICC, 2013, pp. 23–27.

[14] “Hydration of Portland Cement.” https://www.engr.psu.edu/ce/courses/ce584/concrete/library/construction/curing/Hydration.htm (accessed May 17, 2023).

[15] “Ettringite Formation and the Performance of Concrete.” Portland Cement Association, 2001. [Online]. Available: https://www.cement.org/docs/default-source/fc_concrete_technology/is417-ettringite-formation-and-the-performance-of-concrete.pdf?sfvrsn=412%26sfvrsn=412

[16] R. Alizadeh, J. J. Beaudoin, and L. Raki, “Mechanical properties of calcium silicate hydrates,” *Mater. Struct.*, vol. 44, no. 1, pp. 13–28, Jan. 2011, doi: 10.1617/s11527-010-9605-9.

[17] Isa Yuksel, “Blast-furnace slag,” in *Waste and Supplementary Cementitious Materials in Concrete*, Rafat Siddique and Paulo Cachim, Eds., 2018, pp. 361–415. [Online]. Available: https://doi.org/10.1016/B978-0-08-102156-9.00012-2

[18] B. W. Langan, K. Weng, and M. A. Ward, “Effect of silica fume and fly ash on heat of hydration of Portland cement,” *Cem. Concr. Res.*, vol. 32, no. 7, pp. 1045–1051, Jul. 2002, doi: 10.1016/S0008-8846(02)00742-1.

[19] V. Saraswathy and H.-W. Song, “Evaluation of corrosion resistance of Portland pozzolana cement and fly ash blended cements in pre-cracked reinforced concrete slabs under accelerated testing conditions,” *Mater. Chem. Phys.*, vol. 104, no. 2–3, pp. 356–361, Aug. 2007, doi: 10.1016/j.matchemphys.2007.03.033.

[20] T. Yen, T.-H. Hsu, Y.-W. Liu, and S.-H. Chen, “Influence of class F fly ash on the abrasion–erosion resistance of high-strength concrete,” *Constr. Build. Mater.*, vol. 21, no. 2, pp. 458–463, Feb. 2007, doi: 10.1016/j.conbuildmat.2005.06.051.

[21] Y. Ban *et al.*, “Preparation and Performance of Cement Mortar Reinforced by Modified Bamboo Fibers,” *Polymers*, vol. 12, no. 11, Art. no. 11, Nov. 2020, doi: 10.3390/polym12112650.

[22] O. A. Hisseine, W. Wilson, L. Sorelli, B. Tolnai, and A. Tagnit-Hamou, “Nanocellulose for improved concrete performance: A macro-to-micro investigation for disclosing the effects of cellulose filaments on strength of cement systems,” *Constr. Build. Mater.*, vol. 206, pp. 84–96, May 2019, doi: 10.1016/j.conbuildmat.2019.02.042.

[23] S. Amziane and L. Arnaud, “Bioaggregate-based Building Materials, Applications to Hemp Concrete. ISTE Ltd and John Wiley & Sons.” Inc, 2013.

[24] S. Debnath, R. Ranade, S. Wunder, J. Mccool, K. Boberick, and G. Baran, “Interface effects on mechanical properties of particle-reinforced composites,” *Dent. Mater.*, vol. 20, no. 7, pp. 677–686, Sep. 2004, doi: 10.1016/j.dental.2003.12.001.

[25] M. Jebli, F. Jamin, E. Malachanne, E. Garcia-Diaz, and M. S. El Youssoufi, “Experimental characterization of mechanical properties of the cement-aggregate interface in concrete,” *Constr. Build. Mater.*, vol. 161, pp. 16–25, Feb. 2018, doi: 10.1016/j.conbuildmat.2017.11.100.

[26] S. Omairey, N. Jayasree, and M. Kazilas, “Defects and uncertainties of adhesively bonded composite joints,” *SN Appl. Sci.*, vol. 3, no. 9, p. 769, Sep. 2021, doi: 10.1007/s42452-021-04753-8.

[27] S. Yang, X. Zhongzi, X. Ping, and T. Mingshu, “A new method of enhancing cement-aggregate interfaces, I. Ideal aggregate and its effects on interfacial microstructures,” *Cem. Concr. Res.*, vol. 22, no. 4, pp. 612–620, Jul. 1992, doi: 10.1016/0008-8846(92)90013-L.

[28] J. P. Ollivier, J. C. Maso, and B. Bourdette, “Interfacial Transition Zone in Concrete”.

[29] K. L. Scrivener, A. K. Crumbie, and P. Laugesen, “The Interfacial Transition Zone (ITZ) Between Cement Paste and Aggregate in Concrete,” *Interface Sci.*, vol. 12, no. 4, pp. 411–421, Oct. 2004, doi: 10.1023/B:INTS.0000042339.92990.4c.

[30] J. D. Shane, T. O. Mason, H. M. Jennings, E. J. Garboczi, and D. P. Bentz, “Effect of the Interfacial Transition Zone on the Conductivity of Portland Cement Mortars,” *J. Am. Ceram. Soc.*, vol. 83, no. 5, pp. 1137–1144, Dec. 2004, doi: 10.1111/j.1151-2916.2000.tb01344.x.

[31] E. Chiellini, P. Cinelli, V. I. Ilieva, and M. Martera, “Biodegradable Thermoplastic Composites Based on Polyvinyl Alcohol and Algae,” *Biomacromolecules*, vol. 9, no. 3, pp. 1007–1013, Mar. 2008, doi: 10.1021/bm701041e.

[32] S. Iannace, G. Nocilla, and L. Nicolais, “Biocomposites based on sea algae fibers and biodegradable thermoplastic matrices,” *J. Appl. Polym. Sci.*, vol. 73, no. 4, pp. 583–592, Jul. 1999, doi: 10.1002/(SICI)1097-4628(19990725)73:4<583::AID-APP14>3.0.CO;2-H.

[33] M. Bulota and T. Budtova, “PLA/algae composites: Morphology and mechanical properties,” *Compos. Part Appl. Sci. Manuf.*, vol. 73, pp. 109–115, Jun. 2015, doi: 10.1016/j.compositesa.2015.03.001.

[34] A. Barghini, V. I. Ivanova, S. H. Imam, and E. Chiellini, “Poly-(ε-caprolactone) (PCL) and poly(hydroxy-butyrate) (PHB) blends containing seaweed fibers: Morphology and thermal-mechanical properties,” *J. Polym. Sci. Part Polym. Chem.*, vol. 48, no. 23, pp. 5282–5288, Dec. 2010, doi: 10.1002/pola.24327.

[35] S. Torres, R. Navia, R. Campbell Murdy, P. Cooke, M. Misra, and A. K. Mohanty, “Green Composites from Residual Microalgae Biomass and Poly(butylene adipate-co-terephthalate): Processing and Plasticization,” *ACS Sustain. Chem. Eng.*, vol. 3, no. 4, pp. 614–624, Apr. 2015, doi: 10.1021/sc500753h.

[36] F. M. León-Martínez, P. F. D. J. Cano-Barrita, L. Lagunez-Rivera, and L. Medina-Torres, “Study of nopal mucilage and marine brown algae extract as viscosity-enhancing admixtures for cement based materials,” *Constr. Build. Mater.*, vol. 53, pp. 190–202, Feb. 2014, doi: 10.1016/j.conbuildmat.2013.11.068.

[37] H. Amer Algaifi *et al.*, “Insight into the role of microbial calcium carbonate and the factors involved in self-healing concrete,” *Constr. Build. Mater.*, vol. 254, p. 119258, Sep. 2020, doi: 10.1016/j.conbuildmat.2020.119258.

[38] H.-J. Chen, C.-F. Peng, C.-W. Tang, and Y.-T. Chen, “Self-Healing Concrete by Biological Substrate,” *Mater. 1996-1944*, vol. 12, no. 24, p. 4099, Dec. 2019, doi: 10.3390/ma12244099.

[39] H. M. Jonkers, A. Thijssen, G. Muyzer, O. Copuroglu, and E. Schlangen, “Application of bacteria as self-healing agent for the development of sustainable concrete,” *Ecol. Eng.*, vol. 36, no. 2, pp. 230–235, Feb. 2010, doi: 10.1016/j.ecoleng.2008.12.036.

[40] S. Gwon, Y. C. Choi, and M. Shin, “Effect of plant cellulose microfibers on hydration of cement composites,” *Constr. Build. Mater.*, vol. 267, p. 121734, Jan. 2021, doi: 10.1016/j.conbuildmat.2020.121734.

[41] C. Haoyang, “Algae-Based Carbon Sequestration,” *IOP Conf. Ser. Earth Environ. Sci.*, vol. 120, p. 012011, Mar. 2018, doi: 10.1088/1755-1315/120/1/012011.

[42] N. Zhu, M. Ye, D. Shi, and M. Chen, “Reactive compatibilization of biodegradable poly(butylene succinate)/Spirulina microalgae composites,” *Macromol. Res.*, vol. 25, no. 2, pp. 165–171, Feb. 2017, doi: 10.1007/s13233-017-5025-9.

[43] M.-Y. Lin, P. Grandgeorge, A. M. Jimenez, B. H. Nguyen, and E. Roumeli, “Long-Term Hindrance Effects of Algal Biomatter on the Hydration Reactions of Ordinary Portland Cement,” *ACS Sustain. Chem. Eng.*, p. acssuschemeng.2c07539, May 2023, doi: 10.1021/acssuschemeng.2c07539.

[44] X. Chen, M. G. Matar, D. N. Beatty, and W. V. Srubar, “Retardation of Portland Cement Hydration with Photosynthetic Algal Biomass,” *ACS Sustain. Chem. Eng.*, vol. 9, no. 41, pp. 13726–13734, Oct. 2021, doi: 10.1021/acssuschemeng.1c04033.

[45] R. Ramasubramani, R. Praveen, and K. S. Sathyanarayanan, “Study on the strength properties of marine algae concrete,” vol. 9, no. 4, p. 10, 2016.

[46] M. Achenza and L. Fenu, “On Earth Stabilization with Natural Polymers for Earth Masonry Construction,” *Mater. Struct.*, vol. 39, no. 1, pp. 21–27, Aug. 2007, doi: 10.1617/s11527-005-9000-0.

[47] G. Frigione and S. Marra, “RELATIONSHIP BETWEEN PARTICLE SIZE DISTRIBUTION AND COMPRESSIVE STRENGTH IN PORTLAND C~LENT,” *Part. SIZE Distrib.*, vol. 6, no. 1.

[48] D. Vollath, F. D. Fischer, and D. Holec, “Surface energy of nanoparticles – influence of particle size and structure,” *Beilstein J. Nanotechnol.*, vol. 9, pp. 2265–2276, Aug. 2018, doi: 10.3762/bjnano.9.211.

[49] H. Iyer *et al.*, “Fabricating Strong and Stiff Bioplastics from Whole Spirulina Cells”.

[50] C01 Committee, “Specification for Portland Cement,” ASTM International. doi: 10.1520/C0150_C0150M-22.

[51] E29 Committee, “Specification for Woven Wire Test Sieve Cloth and Test Sieves,” ASTM International. doi: 10.1520/E0011-22.

[52] C01 Committee, “Test Method for Compressive Strength of Hydraulic Cement Mortars (Using 2-in. or [50mm] Cube Specimens),” ASTM International. doi: 10.1520/C0109_C0109M-21.

[53] C. A. Schneider, W. S. Rasband, and K. W. Eliceiri, “NIH Image to ImageJ: 25 years of image analysis,” *Nat. Methods*, vol. 9, no. 7, pp. 671–675, Jul. 2012, doi: 10.1038/nmeth.2089.

[54] R. Gabrovšek, T. Vuk, and V. Kaučič, “Evaluation of the Hydration of Portland Cement Containing Various Carbonates by Means of Thermal Analysis,” *Acta Chim Slov*, 2006.

[55] I. Pane and W. Hansen, “Investigation of blended cement hydration by isothermal calorimetry and thermal analysis,” *Cem. Concr. Res.*, vol. 35, no. 6, pp. 1155–1164, Jun. 2005, doi: 10.1016/j.cemconres.2004.10.027.

[56] M. Rupasinghe, R. San Nicolas, P. Mendis, M. Sofi, and T. Ngo, “Investigation of strength and hydration characteristics in nano-silica incorporated cement paste,” *Cem. Concr. Compos.*, vol. 80, pp. 17–30, Jul. 2017, doi: 10.1016/j.cemconcomp.2017.02.011.

[57] S. Ceylan and J. L. Goldfarb, “Green tide to green fuels: TG–FTIR analysis and kinetic study of Ulva prolifera pyrolysis,” *Energy Convers. Manag.*, vol. 101, pp. 263–270, Sep. 2015, doi: 10.1016/j.enconman.2015.05.029.

[58] M. Kazir *et al.*, “Extraction of proteins from two marine macroalgae, Ulva sp. and Gracilaria sp., for food application, and evaluating digestibility, amino acid composition and antioxidant properties of the protein concentrates,” *Food Hydrocoll.*, vol. 87, pp. 194–203, Feb. 2019, doi: 10.1016/j.foodhyd.2018.07.047.

[59] E.-S. Biris-Dorhoi *et al.*, “Macroalgae—A Sustainable Source of Chemical Compounds with Biological Activities,” *Nutrients*, vol. 12, no. 10, p. 3085, Oct. 2020, doi: 10.3390/nu12103085.

[60] N. Wahlström *et al.*, “Cellulose from the green macroalgae Ulva lactuca: isolation, characterization, optotracing, and production of cellulose nanofibrils,” *Cellulose*, vol. 27, no. 7, pp. 3707–3725, May 2020, doi: 10.1007/s10570-020-03029-5.

[61] K. Kumar *et al.*, “Recent developments on biofuels production from microalgae and macroalgae,” *Renew. Sustain. Energy Rev.*, vol. 65, pp. 235–249, Nov. 2016, doi: 10.1016/j.rser.2016.06.055.

[62] A. B. Abell, K. L. Willis, and D. A. Lange, “Mercury Intrusion Porosimetry and Image Analysis of Cement-Based Materials,” *J. Colloid Interface Sci.*, vol. 211, no. 1, pp. 39–44, Mar. 1999, doi: 10.1006/jcis.1998.5986.

[63] F. Moro and H. Böhni, “Ink-Bottle Effect in Mercury Intrusion Porosimetry of Cement-Based Materials,” *J. Colloid Interface Sci.*, vol. 246, no. 1, pp. 135–149, Feb. 2002, doi: 10.1006/jcis.2001.7962.

[64] I. Odler, “The BET-specific surface area of hydrated Portland cement and related materials,” *Cem. Concr. Res.*, vol. 33, no. 12, pp. 2049–2056, Dec. 2003, doi: 10.1016/S0008-8846(03)00225-4.

[65] S. Brunauer, P. H. Emmett, and E. Teller, “Adsorption of Gases in Multimolecular Layers,” *J. Am. Chem. Soc.*, vol. 60, no. 2, pp. 309–319, Feb. 1938, doi: 10.1021/ja01269a023.